Real-time Rendering of Layered Materials with Anisotropic Normal Distributions

Tomoya Yamaguchi
Waseda University
tomoya.tomoya@akane.waseda.jp

Tatsuya Yatagawa
The University of Tokyo
tatsy@den.t.u-tokyo.ac.jp

Yusuke Tokuyoshi
SQUARE ENIX CO., LTD. (now at Intel Corporation)
yusuke.tokuyoshi@gmail.com

Shigeo Morishima
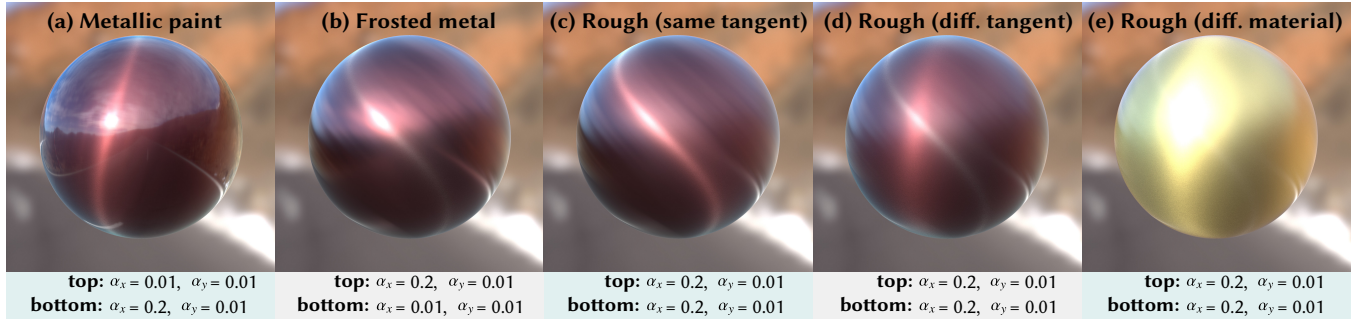Waseda University
shigeo@waseda.jp

Figure 1: Layered materials rendered using the proposed method. Each layer of the materials has an anisotropic normal distribution function (NDF), and it can be defined on a tangent vector field, which differs from layer to layer. The materials are comprised of dielectric top layers with a refractive index of 1.49 **for (a)–(e), and metallic bottom layers with a complex refractive index of** $(1 + 1i, 1 + 0i, 1 + 0i)$ **for (a)–(d) and** $(0.143 + 3.983i, 0.373 + 2.387i, 1.444 + 1.602i)$ **for (e).**

ABSTRACT

This paper proposes a lightweight bidirectional scattering distribution function (BSDF) model for layered materials with anisotropic reflection and refraction properties. In our method, each layer of the materials can be described by a microfacet BSDF using an anisotropic normal distribution function (NDF). Furthermore, the NDFs of layers can be defined on tangent vector fields, which differ from layer to layer. Our method is based on a previous study in which isotropic BSDFs are approximated by projecting them onto base planes. However, the adequateness of this previous work has not been well investigated for anisotropic BSDFs. In this paper, we demonstrate that the projection is also applicable to anisotropic BSDFs and that they can be approximated by elliptical distributions using covariance matrices.

CCS CONCEPTS

• **Computing methodologies** → **Rendering**; **Reflectance modeling**.

KEYWORDS

layered materials, microfacet BSDF, real-time rendering

1 INTRODUCTION

In the last several decades, the visual quality of computer graphics has improved significantly due to the long-standing efforts of both the research and industrial communities. In particular, success in reflectance modeling has enabled representation of a surprisingly wide variety of real-world materials in computer graphics. Among such materials, those comprising of thin layers of different material components have attracted much attention recently due to the demand for surface-painted man-made objects. For example, a car body is coated multiple times with different types of paints, and this process generates a characteristic appearance for the car.

While accurate representation [Jakob et al. 2014; Zeltner and Jakob 2018] and path sampling [Guo et al. 2018] for layered materials have been proposed in the context of offline rendering, light transport in layered materials is usually approximated using analytic models particularly in real-time rendering. Weidlich and Wilkie [2007] and the extension of their work by Elek [2010] linearly combined the bidirectional scattering distribution functions

(BSDFs) of layers using a transmission factor. Guo et al. [2017] extended normal distribution functions (NDFs) using von Mises−Fisher (vMF) distributions to consider multiple reflection lobes and internal scattering. However, the vMF distributions cannot capture the heavy tails of directional distributions, which is often required for modeling metallic materials. Recently, Belcour [2018] considered directional statistics of light rays and formulated how each layer changes the statistics. They referred to the operators that change the statistics as *atomic operators*. Although the atomic operator was practically simple and powerful, its applicability to anisotropic reflection and refraction has not been well investigated. In this paper, we extend the atomic operator for anisotropic reflection and refraction properties of layers.

1.1 Background

In the original method [Belcour 2018], a behavior of light interaction with layered materials was represented by energy of light e and two statistical parameters, that is, the mean $\mu \in [-1, 1]^2$ and variance $\sigma \in [0, \infty]$ of the distribution of light directions[1]. The property of a surface between two neighboring layers is defined by three functions each of which modifies one of the three parameters above. For rough reflection and refraction, the parameters are transformed as follows:

$$e^R = e_i \times FGD^\infty, \ \ \mu^R = -\mu_i, \ \ \sigma^R = \sigma_i + h(\alpha), \tag{1}$$

$$e^T = e_i \times \left(1 - FGD^\infty\right), \ \ \mu^T = -\eta\mu_i, \ \ \sigma^T = \frac{\sigma_i}{\eta} + h(s \times \alpha), \tag{2}$$

$$\text{where} \quad h(\alpha) = \frac{\alpha^{1.1}}{1 - \alpha^{1.1}}, \quad s = \frac{1}{2}\left[1 + \eta\frac{\omega_i \cdot \mathbf{n}}{\omega_t \cdot \mathbf{n}}\right],$$

where $\omega_i \in S^2$ denotes an incident direction; $\omega_t \in S^2$ refers to a refracted direction; $\mathbf{n} \in S^2$ denotes a surface normal; (e_i, μ_i, σ_i) refers to the parameters of incident light; $(e^{\{R,T\}}, \mu^{\{R,T\}}, \sigma^{\{R,T\}})$ denote the parameters of reflected or transmitted light; $\alpha \in [0, 1]$ and η refers to the roughness parameter and relative refractive index on a boundary surface between layers, respectively. FGD^∞ represents the effects of the Fresnel term, shadowing-masking function, and NDF. In the original method, Belcour [2018] precomputed the FGD^∞ values while considering multiple scattering effects [Heitz et al. 2016] and stored them in a lookup table. For detailed definitions of these parameters as well as those for function $h(\alpha)$ and roughness scaling factor s, refer to the original paper [Belcour 2018].

By successively applying the above transformations by the layers, we can obtain e_q, μ_q, and σ_q of outgoing light for a configuration q of successive light interactions. For instance, $q = TRT$ represents a transmission-reflection-transmission path. Let Q be a set of valid sequences of light interactions. Then, a bidirectional reflectance distribution function (BRDF) ρ is defined as follows:

$$\rho(\omega_i, \omega_o) = \sum_{q \in Q} e_q \rho_q(\omega_q, \omega_o, \alpha_q), \tag{3}$$

$$\text{where} \quad \alpha_q = h^{-1}(\sigma_q), \quad \omega_q = \text{reflect}(\mu_q),$$

$$\rho_q(\omega_q, \omega_o, \alpha_q) = \frac{D(\mathbf{h})G(\omega_q, \omega_o)}{4|\omega_q \cdot \mathbf{n}||\omega_o \cdot \mathbf{n}|}.$$

---

[1]The symbol σ represents *variance* rather than standard deviation following the original paper [Belcour 2018]
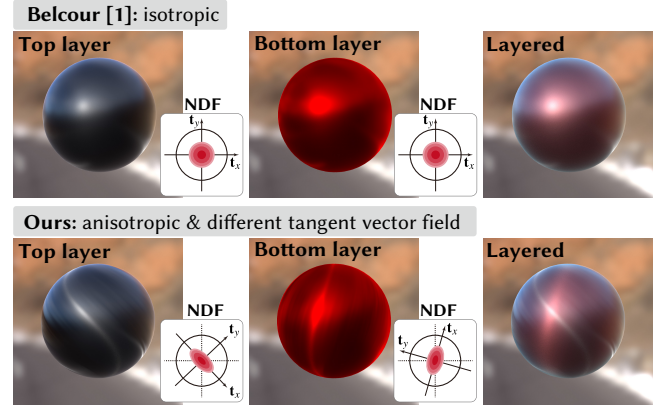

Figure 2: Our method works for layers with anisotropic NDFs defined on varying tangent vector fields, whereas the previous method [Belcour 2018] can be applied only to isotropic NDFs.

In these equations, $\omega_o \in S^2$ is the outgoing direction, $D(\mathbf{h}) \in [0, \infty]$ denotes an NDF for halfvector $\mathbf{h} = (\omega_q + \omega_o)/\|\omega_q + \omega_o\|$, $G(\omega_q, \omega_o) \in [0, 1]$ denotes a shadowing-masking function, and $\text{reflect}(\mu_q)$ represents the direction of perfect reflection for μ_q.

The above formulas are only applicable to isotropic reflection and refraction because the variance is modelled with a single variance parameter σ to define a radially symmetric distribution.

2 LAYERED MATERIALS WITH ANISOTROPIC NORMAL DISTRIBUTIONS

The proposed method is an extension of Belcour's method [2018] which approximated BSDFs by projecting them onto the base plane. The previous study restricted their applicability only to isotropic NDFs. In contrast, the proposed method extends the approach to anisotropic NDFs, as shown in Fig. 2.

2.1 Covariance of Projected Distribution

To represent anisotropic BSDFs projected on the base plane, we employ a 2×2 covariance matrix Σ rather than a scalar variance σ. However, the relationship between the tangent vector field and the covariance matrix is non-trivial. Let $\mathbf{t}_x \in S^1$ and $\mathbf{t}_y \in S^1$ be the tangent and binormal vectors, respectively, that are the orthogonal vectors on the 2D local coordinate system $\mathcal{P}$ of the tangent vector field. When an NDF is projected on the plane, the principal directions of the projected distribution coincide with $\mathbf{t}_x$ and $\mathbf{t}_y$ following the definitions of GGX and Beckmann distributions (see Fig. 3). Because an anisotropic BSDF can be approximated by an anisotropic spherical Gaussian [Xu et al. 2013], its projection to the base plane is also approximated by an anisotropic Gaussian function on the region near to the distribution center, as shown in Fig. 3.

Next, let us consider the relationship between a halfvector $\mathbf{h} = (\omega_i + \omega_o)/\|\omega_i + \omega_o\|$ and outgoing direction ω_o for reflection. Let (x_h, y_h) be the projection of $\mathbf{h}$ in $\mathcal{P}$, and (x_o, y_o) be the projection of ω_o in $\mathcal{P}$. As discussed in a previous study [Stam 2001] (see Appendix B), we assume that $\omega_i = (\sin\theta_i, 0, \cos\theta_i)$ in the tangent space using an incident zenith angle $\theta_i \in [0, \pi/2]$ and an azimuthal
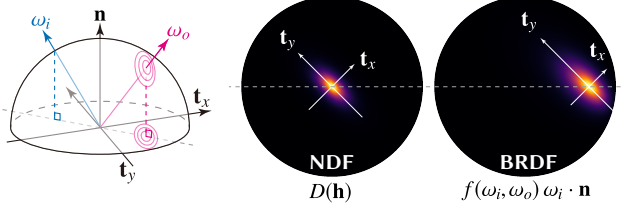
Figure 3: Projected distributions for an NDF and corresponding BRDF are visualized. To evaluate the BRDF, we used the zenith angle $\pi/4$ of incident direction ω_i, as shown in the image to the left. The principal axes for these distributions are the same, and the elliptic shape for the NDF is approximately preserved in that of the BRDF.

angle of zero without loss of generality. Then, the relationship between (x_h, y_h) and (x_o, y_o) can be written as follows:

$$x_o = 2\left(x_h \sin\theta_i + \cos\theta_i\sqrt{1 - x_h^2 - y_h^2}\right)x_h - \sin\theta_i,$$

$$y_o = 2\left(x_h \sin\theta_i + \cos\theta_i\sqrt{1 - x_h^2 - y_h^2}\right)y_h.$$

Thus, the Jacobian matrix $\mathbf{J}_r$ for the coordinate transform from (x_h, y_h) to (x_o, y_o) will be

$$\mathbf{J}_r = \begin{bmatrix} 4x_h\sin\theta_i + \frac{2\left(1 - 2x_h^2 - y_h^2\right)\cos\theta_i}{\sqrt{1 - x_h^2 - y_h^2}} & -\frac{2x_h y_h \cos\theta_i}{\sqrt{1 - x_h^2 - y_h^2}} \\ 2y_h\sin\theta_i - \frac{2x_h y_h \cos\theta_i}{\sqrt{1 - x_h^2 - y_h^2}} & 2x_h\sin\theta_i + \frac{2\left(1 - x_h^2 - 2y_h^2\right)\cos\theta_i}{\sqrt{1 - x_h^2 - y_h^2}} \end{bmatrix}.$$

Assuming x_h, y_h, and θ_i are small enough so that we can ignore the second- and higher-order terms of x_h, y_h, and $\sin\theta_i$, we approximate the above Jacobian matrix as

$$\mathbf{J}_r \approx \begin{bmatrix} 2\cos\theta_i & 0 \\ 0 & 2\cos\theta_i \end{bmatrix}. \tag{4}$$

The same representation was derived by Stam [2001] as an exact solution at the perfect reflection vector (which corresponds to $\boldsymbol{\mu}^R$). Unlike his solution, Eq. (4) is the approximation over the region near $\boldsymbol{\mu}^R$. For refraction, we also approximate the Jacobian matrix $\mathbf{J}_t$ using the same assumption, as follows:

$$\mathbf{J}_t \approx \begin{bmatrix} (\cos\theta_i - \cos\theta_t)/\eta & 0 \\ 0 & (\cos\theta_i - \cos\theta_t)/\eta \end{bmatrix}, \tag{5}$$

where θ_t is the zenith angle for the direction of refraction ω_t. For both cases, the Jacobian matrix is a simple scaling matrix. For the derivation, please refer to the supplementary document.

Although the assumption of the small zenith angle θ_i causes a large error in the grazing angle, we prioritize the simplicity of implementation over physical strictness. While this problem of the grazing angle was also observed in the previous study [Belcour 2018], a compromise is allowable in practice, as we demonstrate later. We also need to consider the effects of the Fresnel term, shadowing-masking function, and cosine term to define a BSDF [Walter et al. 2007]. Nevertheless, these effects are low-frequency and can be negligible when the roughness parameters are relatively small. Therefore, we discuss the property of the coordinate transform using the above Jacobian matrices.

As we can see in Eqs. (4) and (5), the Jacobian matrices for both reflection and refraction are diagonal, and their two diagonal entries are equal. The diagonality implies that the directions of the orthogonal basis vectors of $\mathcal{P}$ are preserved, as shown in Fig. 3. Therefore, we only need to transform anisotropic roughness parameters $(\alpha_x, \alpha_y) \in [0, 1]^2$ along the tangent vector $\mathbf{t}_x$ and binormal vector $\mathbf{t}_y$ to define a covariance matrix for the projected BSDF. The uniformity of the diagonal entries implies that the stretch of the variances along $\mathbf{t}_x$ and $\mathbf{t}_y$ depend on neither the definition of the tangent vector field nor the difference in the roughness parameters. Therefore, we transform the roughness parameters (α_x, α_y) to corresponding scalar variances $(\sigma_x, \sigma_y) \in [0, \infty]^2$ using $h(\alpha)$. Accordingly, the covariance matrix for a BSDF is given as

$$\Sigma = \begin{bmatrix} \mathbf{t}_x & \mathbf{t}_y \end{bmatrix}^\top \begin{bmatrix} \sigma_x & 0 \\ 0 & \sigma_y \end{bmatrix} \begin{bmatrix} \mathbf{t}_x & \mathbf{t}_y \end{bmatrix},$$

where $\quad \sigma_{\{x,y\}} = \begin{cases} h\left(\alpha_{\{x,y\}}\right) & \text{for reflection,} \\ h\left(s \times \alpha_{\{x,y\}}\right) & \text{for refraction.} \end{cases}$

For energy e and mean $\boldsymbol{\mu}$, we use the same representations as those in the previous study because the anisotropy of BSDFs does not affect these terms significantly. Therefore, we obtain an extended BSDF with anisotropic NDFs by substituting the above covariance matrix Σ into Eqs. (1) and (2). To build a *global* BRDF using the adding-doubling method as in the original paper [Belcour 2018], we take exactly the same procedure introduced in it.

3 RESULTS AND DISCUSSION

The following experiments were conducted on a computer with Intel® Core™ i7-8700 3.2 GHz CPU and NVIDIA® GeForce® RTX 2080 Ti GPU. We use a two-layer material in which the bottom conductor layer is coated with a clear dielectric layer. The formulas for two-layer materials are obtained by the adding-doubling method and appear in the supplementary document. We implement the proposed method using Marmoset Toolbag 3 [2019].

In the rendering pipeline, we follow an approximation for FGD^∞ in the implementation of Unity [2019] to avoid the lookup table being memory consuming for anisotropic materials. In addition, we calculate an average covariance matrix, which can differ from channel to channel, for three color channels following the public implementation of the previous works [Belcour 2018; Unity Technologies 2019]

While we mainly show the results of image-based lighting, the computation time of our method for a trivial scene with a directional light is 1.01 ms, which is sufficiently short for real-time applications such as interactive material editing.

Figure 1 shows the rendering results obtained using our method for various layered materials with isotropic/anisotropic NDFs defined on same/different tangent vector fields. These results include only direct illumination from environment maps. For this image-based lighting, we compute the Monte Carlo integration using a visible NDF importance sampling technique [Heitz 2018] for each term of Eq. (3). We compare the computation time between Belcour's method [2018] for isotropic BSDFs and our extension to anisotropic BSDFs. In this comparison, we evaluate both methods by sampling the BRDFs in Eq. (3) separately to focus on the overhead incurred by
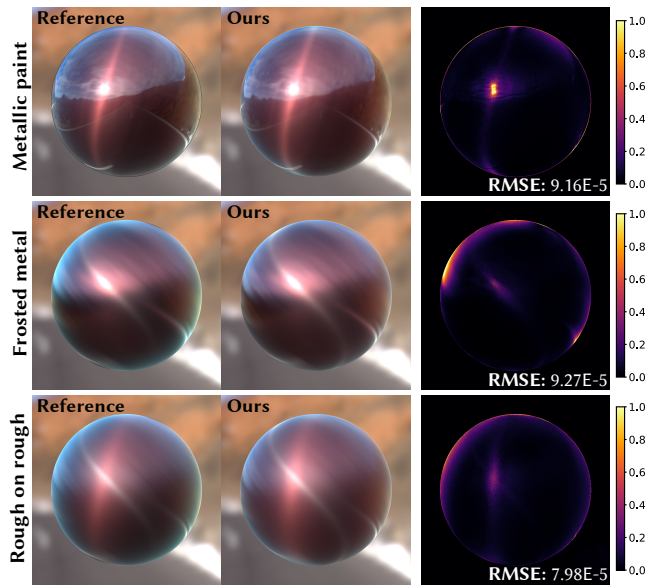
Figure 4: Our results are visually compared with the reference images, and the error value for each pixel is also visualized in the images to the right. The root mean square error (RMSE) values are shown to the bottom left. The roughness parameters for these results are the same as those used for Fig. 1(a), (b), and (d).
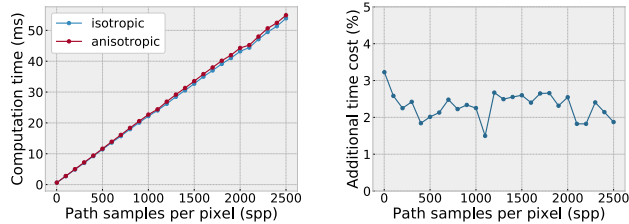

Figure 5: The chart to the left compares the computation time of Belcour [2018] for isotropic BSDFs and our extension to anisotropic BSDFs. The chart to the right shows the additional computation time in percentage terms of our extension over Belcour's method.

changing scalar variance σ to our covariance matrix Σ. Fig. 5 shows the rendering time using varying numbers of samples. Although our method increases the ALU overhead and register pressure, this experimental result demonstrates that the performance degradation when using the method for isotropic BSDFs is negligible.

The visual comparison of the results is shown in Fig. 4. In this figure, pixel-wise root mean square errors (RMSEs) are visualized in the column to the right. We find that the RMSEs are rather large on the rim regions of the sphere, where the viewing angles are comparatively small. However, the overall computation time to render a single frame with 2048 spp was 587.8 ms for naive simulation to obtain reference images, whereas that for our method is only 45.1 ms. Additional results using different roughness parameters

and rotation angles for the local coordinate system appear in the supplementary document.

While our method renders anisotropic layered materials in interactive frame rates by extending Belcour's method [2018], it is inevitable that our method inherits the limitations of this previous method. For example, for layers with very high roughness and indexes of refraction, the directional distributions projected on the base plane may not be elliptical. Despite this fact, the wide applicability of our method to a broad range of layered materials is beneficial to practical graphics production.

4 CONCLUSION

In this paper, we introduced a real-time approach for rendering layered materials wherein the layers are modeled by anisotropic NDFs defined on varying tangent vector fields. The proposed method is easily implemented on the top of the original approach proposed by Belcour [2018] for isotropic NDFs, and is performed with only minor additional computation cost.

ACKNOWLEDGMENTS

REFERENCES

L. Belcour. 2018. Efficient rendering of layered materials using an atomic decomposition with statistical operators. *ACM Trans. Graph.* 37, 4, Article 73 (2018), 15 pages. https://doi.org/10.1145/3197517.3201289

O. Elek. 2010. Layered materials in real-time rendering. In *Central European Seminar on Computer Graphics (CESCG)*.

J. Guo, J. Qian, Y. Guo, and J. Pan. 2017. Rendering thin transparent layers with extended normal distribution functions. *IEEE Trans. on Visualization and Computer Graphics* 23, 9 (2017), 2108–2119. https://doi.org/10.1109/TVCG.2016.2617872

Y. Guo, M. Hašan, and S. Zhao. 2018. Position-free Monte Carlo simulation for arbitrary layered BSDFs. *ACM Trans. Graph.* 37, 6, Article 279 (2018), 14 pages. https://doi.org/10.1145/3272127.3275053

E. Heitz. 2018. Sampling the GGX distribution of visible normals. *Journal of Computer Graphics Tools* 7, 4 (2018), 1–13. http://jcgt.org/published/0007/04/01/

E. Heitz, J. Hanika, E. d'Eon, and C. Dachsbacher. 2016. Multiple-scattering microfacet BSDFs with the Smith model. *ACM Trans. Graph.* 35, 4, Article 58 (2016), 14 pages. https://doi.org/10.1145/2897824.2925943

W. Jakob, E. d'Eon, O. Jakob, and S. Marschner. 2014. A comprehensive framework for rendering layered materials. *ACM Trans. Graph.* 33, 4, Article 118 (2014), 14 pages. https://doi.org/10.1145/2601097.2601139

Marmoset LLC. 2019. Marmoset Toolbag 3. https://marmoset.co/toolbag/

J. Stam. 2001. An illumination model for a skin layer bounded by rough surfaces. In *Eurographics Workshop on Rendering*. 39–52. https://doi.org/10.2312/EGWR/EGWR01/039-052

Unity Technologies. 2019. Unity Scriptable Render Pipeline. https://github.com/Unity-Technologies/ScriptableRenderPipeline/

B. Walter, S. Marschner, H. Li, and K. Torrance. 2007. Microfacet models for refraction through rough surfaces. In *Rendering Techniques*. 195–206. https://doi.org/10.2312/EGWR/EGSR07/195-206

A. Weidlich and A. Wilkie. 2007. Arbitrarily layered micro-facet surfaces. In *Proc. of Int'l Conf. on Computer Graphics and Interactive Techniques in Australia and Southeast Asia (GRAPHITE)*. 171–178. https://doi.org/10.1145/1321261.1321292

K. Xu, W. Sun, Z. Dong, D. Zhao, R. Wu, and S. Hu. 2013. Anisotropic spherical Gaussians. *ACM Trans. Graph.* 32, 6, Article 209 (2013), 11 pages. https://doi.org/10.1145/2508363.2508386

T. Zeltner and W. Jakob. 2018. The layer laboratory: a calculus for additive and subtractive composition of anisotropic surface reflectance. *ACM Trans. Graph.* 37, 4, Article 74 (2018), 14 pages. https://doi.org/10.1145/3197517.3201321